6-1-2021

The observable supernova rate in galaxy–galaxy lensing systems with the TESS satellite

Benne Holwerda
University of Louisville, benne.holwerda@louisville.edu

S Knabel

R C. Steele

L Strolger

J Kielkopf

See next page for additional authors

Original Publication Information

B W Holwerda, S Knabel, R C Steele, L Strolger, J Kielkopf, A Jacques, W Roemer, The observable supernova rate in galaxy–galaxy lensing systems with the *TESS* satellite, *Monthly Notices of the Royal Astronomical Society*, Volume 505, Issue 1, July 2021, Pages 1316–1323,

Monthly Notices of the ROYAL ASTRONOMICAL SOCIETY

MNRAS **505,** 1316–1323 (2021) https://doi.org/10.1093/mnras/stab1370
Advance Access publication 2021 May 13

The observable supernova rate in galaxy–galaxy lensing systems with the *TESS* satellite

B. W. Holwerda [1]★ S. Knabel,[1]★ R. C. Steele,[1] L. Strolger,[2] J. Kielkopf,[1] A. Jacques[1] and W. Roemer[1]

[1]*Department of Physics and Astronomy, University of Louisville, 102 Natural Science Building, Louisville, KY 40292, USA*
[2]*Space Telescope Science Institute, 3700 San Martin Dr, Baltimore, MD 21218, USA*

Accepted 2021 April 23. Received 2021 April 21; in original form 2020 June 30

ABSTRACT

The *Transiting Exoplanet Survey Satellite* (*TESS*) is the latest observational effort to find exoplanets and map bright transient optical phenomena. Supernovae (SNe) are particularly interesting as cosmological standard candles for cosmological distance measures. The limiting magnitude of *TESS* strongly constrains SN detection to the very nearby Universe ($m \sim 19$, $z < 0.05$). We explore the possibility that more distant SNe that are gravitationally lensed and magnified by a foreground galaxy can be detected by *TESS*, an opportunity to measure the time delay between light paths and constrain the Hubble constant independently. We estimate the rate of occurrence of such systems, assuming reasonable distributions of magnification, host dust attenuation, and redshift. There are approximately 16 Type Ia SNe (SNIa) and 43 core-collapse SNe (SNcc) expected to be observable with *TESS* each year, which translates to 18 and 43 per cent chance of detection per year, respectively. Monitoring the largest collections of known strong galaxy–galaxy lenses from Petrillo et al., this translates into 0.6 and 1.3 per cent chances of an SNIa and an SNcc per year. The *TESS* all-sky detection rates are lower than those of the Zwicky Transient Facility and Vera Rubin Observatory. However, on the ecliptic poles, *TESS* performs almost as well as its all-sky search, thanks to its continuous coverage: 2 and 4 per cent chance of an observed SN (Ia or cc) each year. These rates argue for timely processing of full-frame *TESS* imaging to facilitate follow-up and should motivate further searches for low-redshift lensing system.

Key words: gravitational lensing: strong – surveys – galaxies: elliptical and lenticular, cD – distance scale – transients: supernovae.

1 INTRODUCTION

The *Transient Exoplanets Survey Satellite* (*TESS*; Ricker et al. 2015) is an outstanding tool for exploring transient phenomena, such as supernovae on cosmological distance scales, in its all-sky survey. However, the limiting depth of the 2-min or 30-minute (integrated) cadence on each sector limits the volume of the Universe that can be probed using *TESS*.

Fortunately, there are many galaxy–galaxy strong gravitational lenses that can magnify more distant supernovae. Traditionally, these have been found mostly in spectroscopic surveys such as the Sloan Digital Sky Survey (SDSS; Abazajian et al. 2003; Abolfathi et al. 2018) and the Galaxy and Mass Assembly (GAMA) survey (Driver et al. 2009; Liske et al. 2015; Baldry et al. 2018). Because the signals from both the lens and more distant source galaxy are present in a single fibre spectrum, one can identify these as blended spectra as well as estimate the redshifts of both galaxies (lens and source). The clean selection through blended spectra has resulted in a very high confirmation rate for programs based on this technique: the SLACS, BELLS, and SLACS4MASSES surveys (Bolton et al. 2006; Treu et al. 2006; Koopmans et al. 2006; Gavazzi et al. 2007; Bolton et al. 2008a; Gavazzi et al. 2008; Bolton et al. 2008b; Treu et al. 2009; Auger et al. 2009, 2010; Newton et al. 2011; Shu et al. 2015) and ongoing searches using GAMA (Holwerda et al. 2015b; Knabel et al. 2020).

However, the selection function for these gravitational lenses is a convolution of the spectroscopic target selection and whether the fibre encloses the Einstein ring of the gravitational lens. Hence, while they select clean samples, the on-sky number of strong gravitational lenses is more difficult to estimate (e.g. Knabel et al. 2020).

Enter large-scale gravitational lens identification, either through citizen science such as the GalaxyZoo (Lintott et al. 2008) or machine-learning techniques. The latter has been particularly successful using a training set generated using existing elliptical galaxies with added lensed arcs as the training set (Petrillo et al. 2017, 2018; Li et al. 2020). In their application using the (colour) images of the 1500 deg^2 Kilo-Degree Survey (KiDS; de Jong et al. 2013, 2015, 2017), Petrillo et al. (2019) found 1300 such gravitational lenses and a similar number was discovered in the Dark Energy Survey (DES; Jacobs et al. 2019; Huang et al. 2020, 2021).

Interest in lensed supernovae and other bright transient phenomena is particularly high at the moment because the time differences between observed lensed supernova images (due to the different paths taken by light through the lensing galaxy) are sensitive to the expansion rate of the Universe. Refsdal (1964) proposed to measure the value of the Hubble constant (H_0) from the time delays of multiply

★ E-mail: benne.holwerda@gmail.com, Benne.holwerda@louisville.edu (BWH); shawnknabel@gmail.com (SK)

imaged SNe (for excellent reviews, see Treu & Marshall 2016; Oguri 2019).

Since the discovery of a multiply imaged supernova (appropriately named Refsdal, see Kelly et al. 2015a, b, c), the feasibility of measuring the value of H_0 with this method became possible (Vega-Ferrero et al. 2018). An independent H_0 measurement would be timely given the recent discrepancy of the H_0 value measured by the two dominant independent cosmological probes – the cosmic microwave background (Planck Collaboration 2020) and local distance ladders (Beaton et al. 2016; Riess et al. 2016, 2018; Riess 2019).

The possibility of a strongly lensed supernova has now gone from an early possibility (Wang 2000; Porciani & Madau 2000; Goobar et al. 2002b, a; Holz 2001; Kostrzewa-Rutkowska, Wyrzykowski & Jaroszyński 2013) to a realistic prospect to be detected in statistical samples with modern survey cadence and sensitivity. Strongly lensed supernova in galaxy–galaxy lenses has been reported in iPTF, a precursor to the Zwicky Transient Factory (Goobar et al. 2017), and in Pan-STARRS (Quimby et al. 2014).

Interest is now moving to how near-future observatories (e.g. *JWST*; Petrushevska et al. 2018), VRO/LSST (Liao 2018; Tu, Hu & Wang 2019), and other time-domain surveys (Goldstein, Nugent & Goobar 2019)) can find a transient event in the source galaxy of a strong gravitational lens. Shu et al. (2018) explored the supernova rate (SNR) expected for the SLACS and related programs (BELLS and SLACS4MASSES), given their spectroscopically selected lenses and their source redshift distribution. They show that facilities such as the DES telescope and Vera Rubin Observatory (VRO) can very likely identify lensed supernovae candidates in these surveys.

Our interest is to explore how well *TESS* would be able to detect such transients, either by monitoring known lenses or as a blind survey. Despite the fact that *TESS* limiting depths are much shallower than those considered in Shu et al. (2018), the on-sky density of lensing galaxies from Petrillo's result indicates that there could be a useful number of supernova detections via lensed sources observed in the current and future *TESS* mission. The high cadence and 27-d-long light curves of *TESS* open the possibility of observing the SNIa light curve as it occurs in multiple images of the lensed source. The continuous viewing zone for *TESS* at both ecliptic poles offers even better time coverage with 357-d coverage. Our aim in this paper is to explore how much of a scientific return can be expected by building an immediate search for supernova in the *TESS* data for rapid follow-up.

2 ESTIMATING LENSED SN RATES IN *TESS*

We follow the same method demonstrated in Shu et al. (2018), populating the sky with lenses like those found in the Petrillo and other samples, and estimating the supernova rate, the apparent magnitude based on the Shu et al. (2018) magnification distribution (Fig. 1), the absolute magnitude distribution from (Richardson et al. 2014) shown in Fig. 3 and an assumed redshift distribution (Fig. 2) based on the source distribution in Holwerda et al. (2015b) and Shu et al. (2018) combined. We follow the approach in Shu et al. (2018) for the *TESS* estimates by populating N lenses using either supernova type Ia absolute magnitudes and the four core-collapse supernovae types listed in Richardson et al. (2014).[1]

[1]Li et al. (2011) has the more complete fractions of observed types (their fig. 11). For SNe Ia, we focus on the most numerous normal Type Ia, and disregarding rarer and less luminous 91bg and 02cx types.

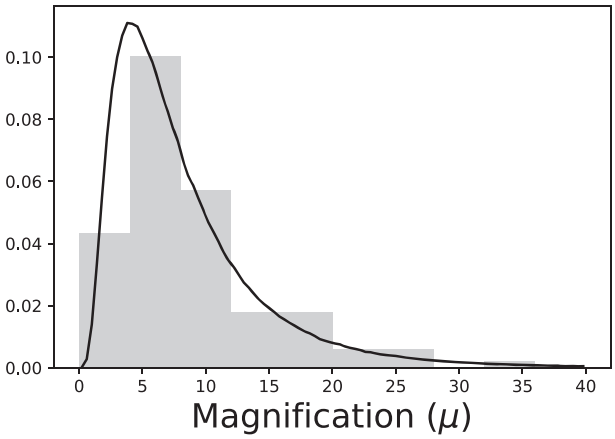

Figure 1. The distribution of magnification by the foreground lensing galaxy of the background source we assume for our estimates. The histogram is the distribution of values in SLACS and the line best description lognormal distribution we use for the estimates.

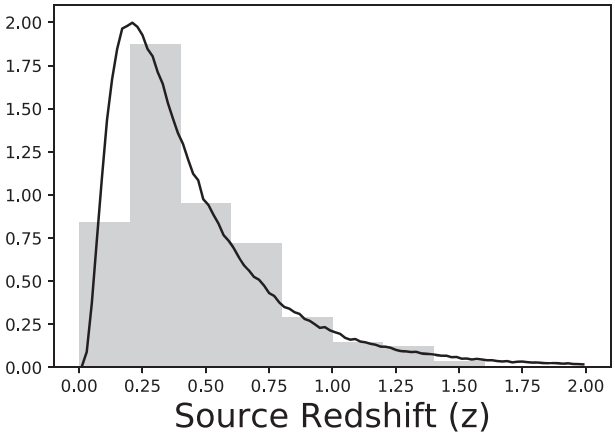

Figure 2. The distribution of source galaxy redshifts assumed for our estimates. This is the combined redshift numbers from SLACS and GAMA (grey histogram) and the best lognormal distribution describing it (solid line).

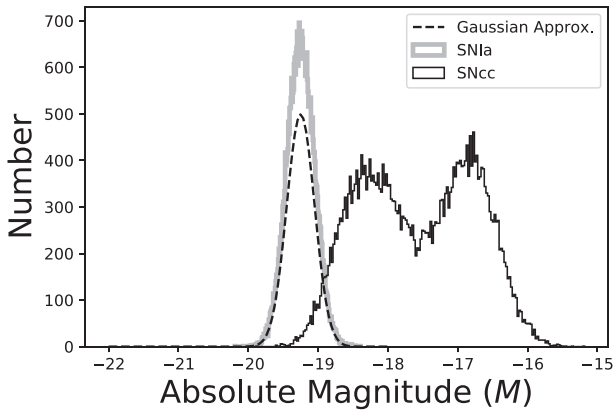

Figure 3. The absolute magnitude distributions of SNIa and core-collapse (Type IIb, IIL, IIP, and IIn combined) based on the values reported in Richardson et al. (2014).

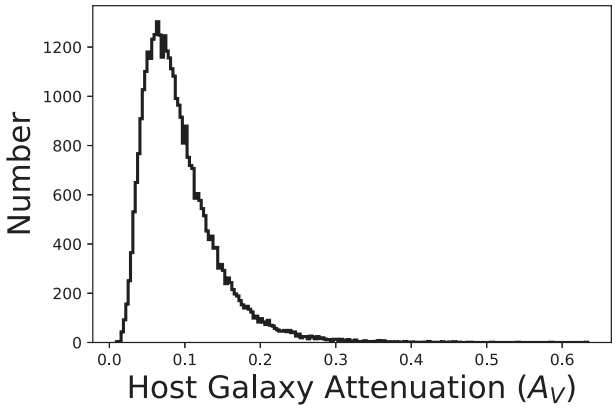

Figure 4. The host galaxy attenuation distribution for a 10^9 $M_\odot$ stellar mass disc galaxy from Holwerda et al. (2015c) based on the *HST* imaging presented in Holwerda et al. (2009). Given the selection criteria for lens selection (blue arcs, implying smaller, star-forming galaxies), we adopt this distribution to randomly draw host attenuation (A_V) values from for each supernova.

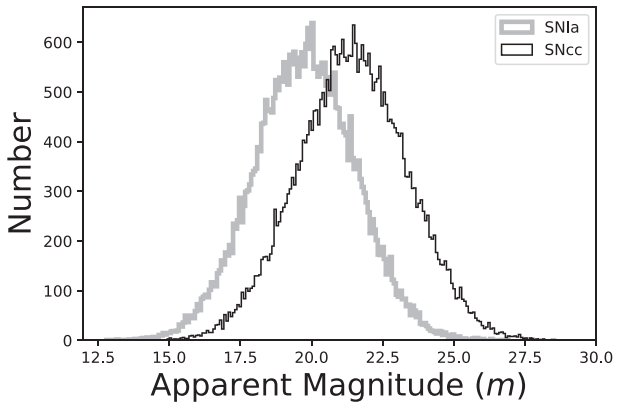

Figure 5. The apparent magnitude distributions of SNIa and core-collapse (Type IIb, IIL, IIP, and IIn combined) after randomly drawing from their absolute magnitude distribution and the redshift and magnification distributions in Figs 1 and 2 and adding host attenuation from Fig. 4.

Drawing from the normal distribution defined by the mean and standard deviation of absolute magnitudes in table 1 of Richardson et al. (2014) and equally randomly drawing from the four distributions for core-collapse supernovae, we obtain the distributions in Fig. 3.

The magnification distribution in Fig. 1 is from Shu et al. (2018) alone, as this is the most uniform sample available. We fit a lognormal distribution ($\mu = 1.9$, $\sigma = 0.7$) to this distribution, which is a reasonable description (K-S = 0.1, $p = 0.05$) using the Kolmogorov–Smirnov test; it deviates a maximum of 10 per cent from the lognormal description.

The redshift distribution in Fig. 2 is drawn from the combination of source redshifts from Shu et al. (2018), Holwerda et al. (2015b), and Knabel et al. (2020). The source redshift distribution from Holwerda et al. (2015b) follows a lognormal distribution (K-S = 0.1, $p = 0.003$), as does the one from Shu et al. (2018) but with much lower significance (K-S = 0.04, $p = 0.98$). The combined sample is reasonably described with a lognormal distribution as well (K-S = 0.06, $p = 0.07$). We adopt the lognormal approximation for the source redshifts ($\mu = -1.04$, $\sigma = 0.75$) to describe the redshift distribution, as it deviates from the lognormal distribution by less than 10 per cent.

As volume increases at higher redshifts, the chances of alignment and strong lensing increase. However, we assume here that the redshift distribution is appropriate for *TESS* detected lensed supernovae as (a) we assume Petrillo-like lenses in the blind survey and (b) the Petrillo ML algorithm was trained on SLACS-like artificial lenses. This assumption does ignore higher redshift ($z > 0.5$) lenses, lensing high-redshift sources ($z \sim 1$) with extreme magnifications. As a result, our estimates for the *TESS* detected supernovae rates are likely slightly underestimated. Knabel et al. (2020) estimated the on-sky density of lenses such as those in SLACS but the combined selection effects will miss strongly lensed events and the estimate of all-sky lensed events presented later are underestimates

To estimate the host galaxy attenuation, we adopt the distribution of A_V values from Holwerda et al. (2015c), shown in Fig. 4, which is based on the overlapping galaxy pair originally described in Holwerda et al. (2009, 2013). From overlapping pairs of galaxies (Domingue, Keel & White 2000; White, Keel & Conselice 2000; Keel & White 2001a, b; Holwerda, Keel & Bolton 2007; Holwerda et al. 2013; Holwerda & Keel 2016), we know there is a wide variety of attenuation distributions depending on stellar mass and positions in the disc of a galaxy. This particular template is for a 10^9 $M_\odot$ stellar mass disc galaxy, which is a reasonably choice for the star-forming galaxies preferred for the source galaxies (lenses are identified in colour images from blue arcs). In effect, host galaxy is both inclination dependent (Holwerda et al. 2015a) and strongly depends on the relative distribution of dust and SN progenitors (Holwerda 2008; Holwerda in preparation).

We now combine the absolute magnitude distribution with the luminosity distances for each redshift, the magnifications and the host attenuation distribution to obtain apparent magnitude distributions for both Type Ia supernovae and core-collapse supernovae. This is effectively convolving the distributions in Fig. 3 with the distributions in Figs 1 and 2 to arrive at the apparent magnitude distribution in Fig. 5. These distributions are close to Gaussian with $m = 19.69 \pm 1.78$ and $m = 21.38 \pm 1.94$ for SNIa and SNcc, respectively; these mean values fall below a reasonable *TESS* limit but have a wide enough spread to potentially be observable.

The on-sky density of strong lenses needs to be estimated as well and this number is not yet well settled. From the initial pass by Petrillo et al. (2019), there is about 0.8 lens deg^{-2}. However, Knabel et al. (2020) estimate a higher on-sky density based on a mix of identification techniques, closer to 1.27 lens deg^{-2} by combining all three identification methods. Even so, this number is likely to be an underestimate. Using the latter as our on-sky density with 70 per cent of the area accessible by *TESS* (due to the Zone of Avoidance and Zodiacal light), we estimate the approximate number of strong lenses in the *TESS* survey to be ∼37 thousand lenses. Starting with an absolute magnitude (Fig. 3), and randomly drawing from the redshift and magnification distributions (Figs 1 and 2), we arrive at the distribution of apparent magnitudes in Fig. 5 in the all-sky lens survey. The redshifts assigned to each random draw can be translated into an SNR for each type using the relation found by Shu et al. (2018).

Shu et al. (2018) estimated the star formation rates (SFRs) in each lensed galaxy in SLACS using the [O II] emission line. The core-collapse supernova rate is directly proportional to the recent SFR (Dahlén & Fransson 1999; Oguri 2010) with a factor for galaxy mass (see Strolger et al. 2015). A similar reasoning can be followed for the SNIa rate (Dahlén & Fransson 1999). We fit a linear relation to the values in the Shu et al. (2018) lenses (colour points in Fig. 6) and populate the all-sky survey based on the drawn redshift and the

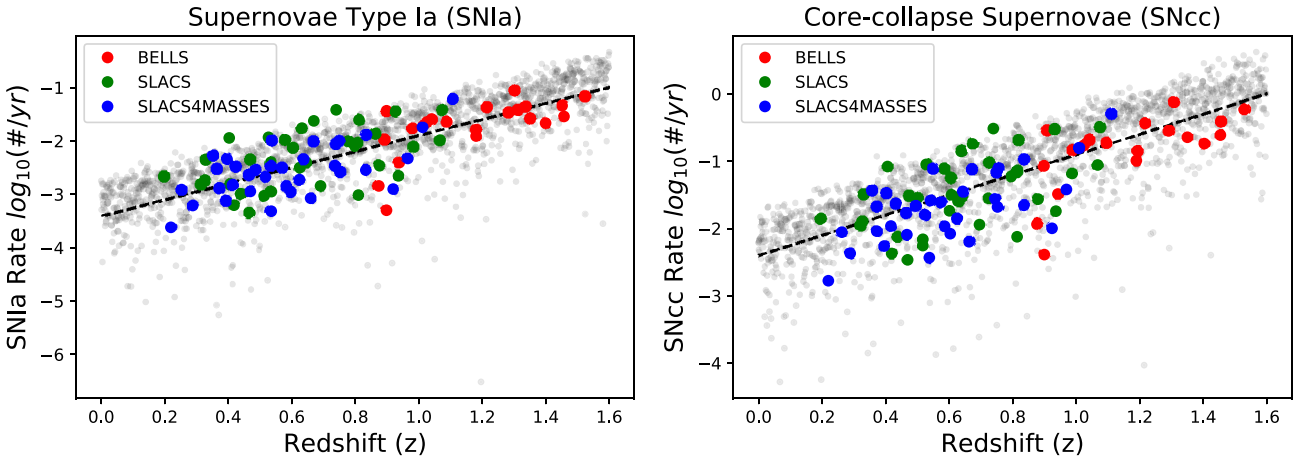

Figure 6. The relation between supernova rates and redshift for SNIa (left) and SNcc (right). The estimated SNIa and SNcc rates from Shu et al. (2018) for the three strong lensing surveys are shown. The dashed line is the best linear fit through these values. We use this fit and the inferred scatter around it to populate the lenses drawn for the *TESS* survey.

variance of SNR at that redshift (grey points in Fig. 6). Please note that this implicitly uses the redshift distribution shown in Fig. 2 for the rates, and that likely higher rates at greater redshift are not fully included in the all-sky estimate.

The supernova rates for both SNIa and SNcc are inferred from the spectroscopic SFR by Shu et al. (2018) for the source galaxies as a function of redshift (Fig. 6).

Starting from the randomly drawn redshift, we populate the target population in both apparent magnitude and the supernova rate. This is visualized in Fig. 7 for both types of supernova under consideration. The rates of occurrence of SNIa that are being lensed by a massive galaxy along the line of sight is relatively low, but because these are brighter to start with (Fig. 5), a sizeable number make it across the fiducial *TESS* detection limit. The core-collapse supernovae start almost two magnitudes dimmer than the SNIa, but are much more common. Their higher occurrence rate pushes them into competitive numbers above the *TESS* detection limit.

To find the total number of lensed supernovae of the two types – SNIa and SNcc – we sum the occurrence rates in Fig. 7 and show these in Fig. 8. Only a few supernovae of both kinds over the whole sky are close enough and magnified enough by the gravitational lenses to be detectable with *TESS*: 16.37 SNIa per year and 44.1 SNcc per year. However, that is a reasonable occurrence rate to start looking for a signal in the *TESS* data of the first 2 yr.

TESS does not monitor the whole sky continuously, but there is considerable overlap between its campaigns as it covers 1/28th of the sky at a time in 27-day periods, completing the full sky in 2 yr. Two 'continuous viewing zones' are on each ecliptic pole, resulting in 357 d coverage of each. There is some overlap between other sectors as well. To first order, this means 1.3 lensed SNIa and 13.4 lensed SNcc are in the *TESS* primary mission data (first 2 yr). This drops to 0.5 SNIa and 6 SNcc if we limit ourselves to $m < 18$ to ensure a good light curve fit. Note that this all-sky estimate was arrived at assuming SLACS-like lenses with source redshifts (Fig. 2) and magnifications (Fig. 1) and higher redshift and magnification events are excluded, underestimating the rate.

In the extended mission of *TESS*, one could consider optimizing the detection rate by *TESS* of these lensed supernovae: longer campaigns to ensure the peak of the light curve is observed, an alert system based on rising sources, and full-frame detections of a supernova.

3 WHY ARE LENSED SNIA SO IMPORTANT?

The occurrence of a supernova in a lensed system is rare, but these are significant opportunities for an independent test of our current understanding of cosmology. Multiple images of the background source galaxy each carry a separate image of the supernova, with a time delay between our observations of each supernova image that is expected to be on the order of days. The exact timing of each image of the supernovae brightening tells us the difference in the length of the path the light took, an independent test of General Relativity, Dark Matter, and Dark Energy. Two supernovae in the source of a strongly lensed galaxy have been reported (Quimby et al. 2014; Goobar et al. 2017). Only one supernova with multiple Hubble imaging has been observed (SN Refsdal; Kelly et al. 2015a), but this *one object*, well characterized, already constrained the universe's cosmology (Vega-Ferrero et al. 2018; Grillo et al. 2018; Williams & Liesenborgs 2019; Pierel & Rodney 2019).

4 DISCUSSION

We made several assumptions in the estimate of the observable supernovae in lensed systems with *TESS*:

(i) The strong lenses identified in Petrillo et al. (2019) are representative and complete for all strong lenses in the sky. This is most likely a complete survey of the most massive and closest lens galaxies (and therefore with most clearly identifiable arcs) but unlikely to be a complete census as more blended systems are inherently missed by the machine-learning algorithm. Their on-sky density of $\sim$0.8 deg^{-2} is therefore an *underestimate*. We adopted the more complete value of 1.27 deg^{-2} from Knabel et al. (2020) to estimate the observation rates.

(ii) The magnification distribution for the on-sky strong lenses is similar to the distribution found by Shu et al. (2018) for the spectroscopically identified lenses, which are limited in diameter on the sky by the spectroscopic fibre of the survey and therefore favour slightly more distant or lower-mass galaxy lenses. Petrillo et al. (2019) show their sample overlaps well with SLACS in mass–redshift space and is therefore likely representative. Thus, the magnifications assumed are likely an *underestimate* of the distribution of all on-sky lenses.

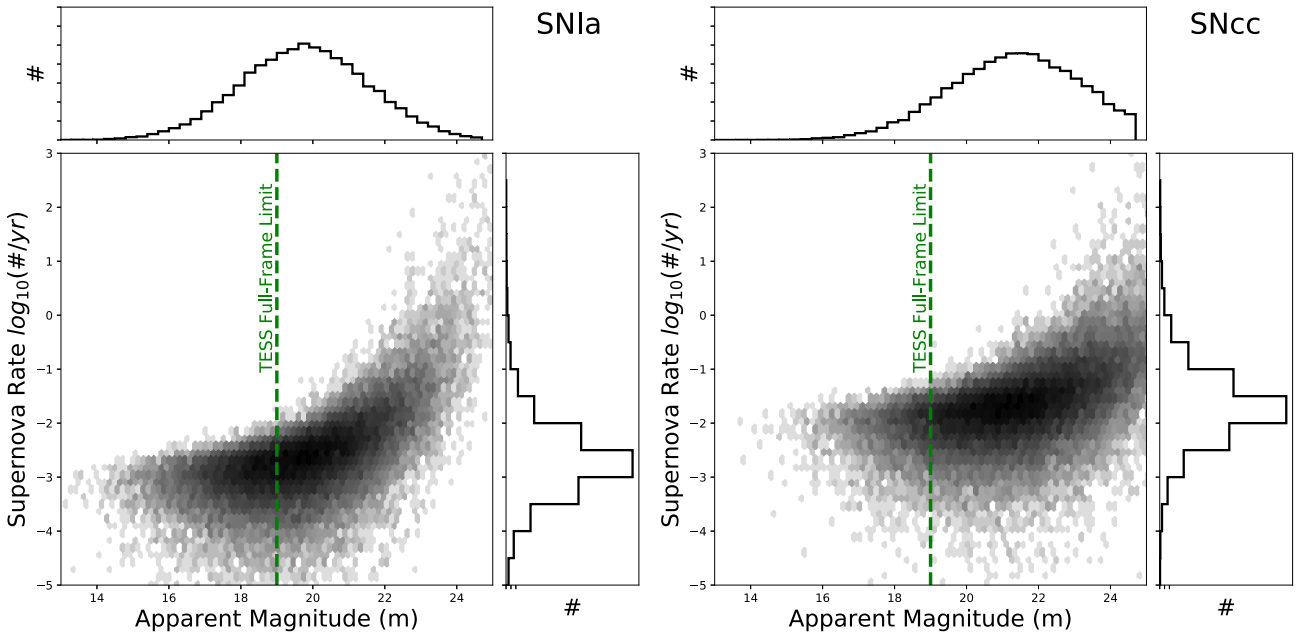

Figure 7. The distribution of apparent magnitudes and supernova rates for an all-sky distribution of strong lenses for both Type Ia and core-collapse supernovae. The parameter space covered is either highly magnified and rare, or common and low magnification.

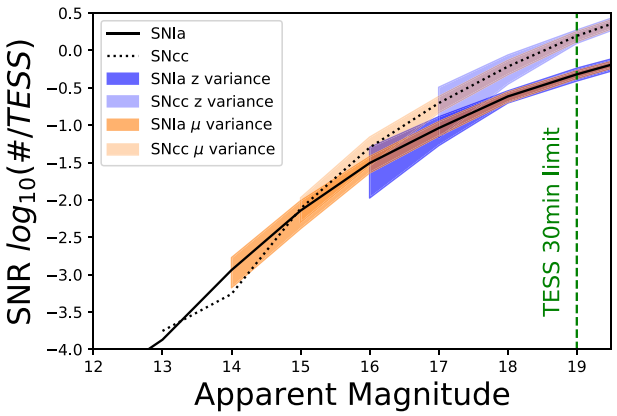

Figure 8. The summed all-sky supernova rate in gravitationally lensed host galaxies as a function of apparent magnitude in bins of 0.5 mag. The figure shows the variance in the redshift distribution of the magnification distribution by 0.1 in peak or tail of the lognormal distribution.

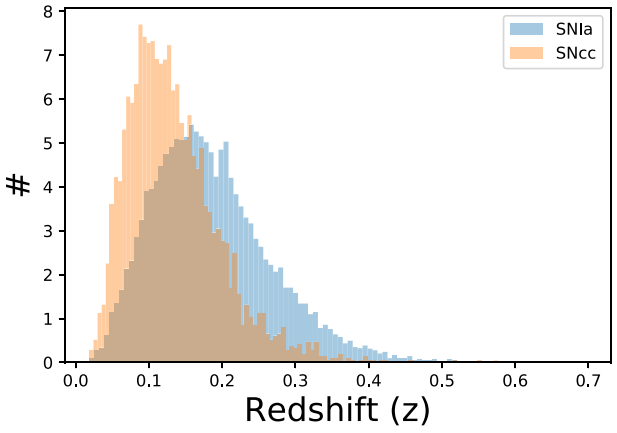

Figure 9. The distribution of SN, SNIa, and SNcc that could be detected by *TESS* ($m < 19$). Both peak before the assumed redshift distribution does (Fig. 2). The source redshift distribution as found from the spectroscopically identified is a good proxy for the redshift distribution of sources whose supernova could be detected with *TESS*.

(iii) The source galaxy redshift distribution from Holwerda et al. (2015b) and Shu et al. (2018) combined is representative of the ones observed all over the sky. These spectroscopically identified lenses are biased towards more distant lenses and hence sources. The redshift distribution may therefore be a slight *overestimate* of the actual on-sky redshift values (cf. Fig. 9). However, higher redshift but strongly magnified events are not considered and this results in a net underestimate of the predicted rate.

(iv) The supernova rates were consequently as high as those in Shu et al. (2018) for star-forming galaxies at higher redshifts. The lensed arcs in Petrillo et al. (2019) are selected by their blue colour and are therefore likely also star-forming galaxies, but – as pointed out above – at lower redshifts. The SNR may therefore be an *overestimate*, thanks to the possible overestimate of the redshift distribution.

(v) The host galaxy attenuation curve is for a smaller star-forming galaxy (Fig. 4; Holwerda et al. 2015c) but supernovae occur in all kinds of galaxies. We assume this is a good approximation of the source galaxies but it may constitute an underestimate of the SNIa's attenuation from the host galaxy.

(vi) We have ignored overlap in *TESS* field coverage (e.g. ecliptic poles) for the estimated all-sky rates. In effect this will improve *TESS*'s odds since there is substantial field overlap (especially in the Northern campaign, see Section 5.1).

Three of our six assumptions cause us to *underestimate* the number of observable supernovae in the *TESS* survey. The overestimate of the supernova rate in the source galaxies and smaller volume may lower the number. Hence, we treat our (approximate) estimate of the lensed supernovae rate as an underestimate for the *TESS* observations.

Fig. 8 shows the variance in the distribution of SNR and apparent magnitude if we vary the redshift distribution in both center and

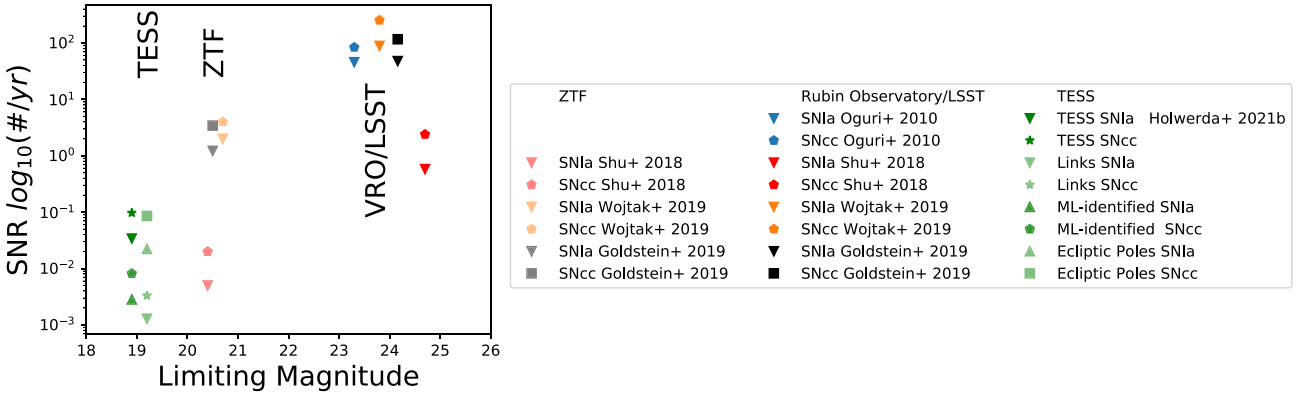

Figure 10. The detection rates for different lensed supernova types for the ZTF and Rubin Observatory/LSST surveys from Oguri & Marshall (2010), Wojtak et al. (2019), Goldstein et al. (2019), and Shu et al. (2018). The green points are different estimates using *TESS* as the survey instrument: all-sky *TESS* detections of lensed supernovae, monitoring the LiNKS machine-learning identified strong lensing systems, monitoring all machine-learning identified strong lensing systems in DES/KiDS/SLACS, etc., and the continuous monitoring of the Ecliptic poles. The *TESS* all-sky and the ecliptic poles blind searches with *TESS* may be competitive in the near-term for all-sky searches for lensed supernovae and will remain competitive in the ecliptic poles, thanks to continuous coverage.

width (Fig. 2). Fig. 8 shows the same variance for changing the distribution of magnifications (Fig. 1). Variance in the redshift or magnification distribution are not substantially different from Fig. 8 and only show stochasticity at the brightest apparent magnitudes. The greatest variance in the distribution occurs with the change in redshift distribution of the source galaxies. This distribution is difficult to predict, which is why we opted for a simple lognormal based on existing data to approximate the distribution observed in Holwerda et al. (2015b) and Shu et al. (2018).

The innovation in strong lensing statistics is happening thanks to machine-learning identification of strong lenses in imaging surveys. Recent efforts such as the KiDS (Petrillo et al. 2017, 2018, 2019) and DES (Jacobs et al. 2019; Huang et al. 2020, 2021) surveys have increased the numbers of known lenses from couple hundred to several thousand. These machine-learning identifications prefer high-mass and closer lens galaxies, making the source arcs more easily identifiable in ground-based images. Knabel et al. (in preparation) confirm several with existing GAMA spectroscopy showing weak second redshift signal because the arcs fall mostly outside the spectroscopic fibre aperture. These are ideal systems for *TESS* to monitor as their magnification is higher and sources are well separated from the lensing galaxy. The on-sky density of these strong galaxy–galaxy lenses go a long way in explaining why a relatively low-redshift supernova such as iPTF16geu (Goobar et al. 2017) can be found with high magnification ($z = 0.2$ lens).

Supernova rates in gravitationally magnified systems are presented in Oguri & Marshall (2010), Shu et al. (2018), Wojtak, Hjorth & Gall (2019), and Goldstein et al. (2019) with a variety of assumptions and for different time-domain surveys. These estimates for ZTF and Rubin Observatory/LSST are shown in Fig. 10 for reference. The majority are for blind searches and a few for monitoring well-known strong lensing samples. *TESS* offers a different approach, monitoring large samples of candidate lenses as well as all-sky or polar blind searches.

Any *TESS* detection in a lensed system offers the possibility to repeat the supernova timing experiment conducted by Kelly et al. (2015a) in a single lensing galaxy instead of a lensing galaxy cluster. Current estimates are for the near-future VRO, but even for that powerful transient observatory, supernovae in lensed system observation rates are of order unity (Goldstein et al. 2019), which makes the *TESS* observations potentially competitive.

5 CONCLUSION

TESS is promising to be an amazing tool for a wide variety of astronomical topics, ranging from the exoplanets it was meant to find to stellar seismology and other transient phenomena. We present here the odds of not only finding a supernova – several have already been discovered by *TESS* in combination with the All-Sky Automated Survey for supernovae (ASAS-SN) see e.g. Vallely et al. (2019) – but aslo an estimate of how many of these have been significantly lensed by a strong gravitational lens of a foreground massive galaxy.

The total number of lensed SNIa and SNcc per year in the *TESS* visibility envelope is proportionally lower, resulting in about 0.5 or 1.3 SNIa and 6 or 13.4 SNcc potentially identifiable (assuming an $m < 18$ or $m < 19$ limiting magnitude) in the *TESS* primary 2-yr mission. Alternatively, one could monitor the KiDS-identified strong lensing systems alone (LiNKS Petrillo et al. 2019). This would lower the expected rates by another order of magnitude in exchange for the certainty that these are lensed supernovae. The odds of finding one each year in the TESS data are approximately 18 and 43 per cent for SNIa and SNcc respectively and 0.6 and 1.3 per cent SNIa and SNcc per year just monitoring already known lenses. With the results from the DES search for strong lenses (Jacobs et al. 2019; Huang et al. 2020, 2021), the total number of known strong lensing galaxies, mostly found through machine learning and worth monitoring, is close to 3000, doubling the numbers for just LiNKS (see Fig. 10).

Fig. 10 shows the *TESS*- and KiDS-monitored supernova rates in comparison to the rates predicted for the Zwicky Transient Facility and the Vera C. Rubin Observatory by Goldstein et al. (2019) and Shu et al. (2018). These are for the full survey (Goldstein et al. 2019) or monitoring known strong lenses (Shu et al. 2018), similar to our proposed *TESS* and KiDS-identified (by Petrillo et al. 2019) strong lenses. The *TESS* numbers are an order of magnitude below the other surveys' expected supernova yields. We note the all-sky *TESS* yield is comparable with the ZTF dedicated lens monitoring (Fig. 10). Monitoring known lenses such as those in the KiDS survey (LinKS, lenses in a square degree Petrillo et al. 2019), similarly yields an order of magnitude fewer supernovae for *TESS*. One viable way

to improve *TESS* (and other transient observatories) performance is to increase the number of known lens systems to monitor. Given that strong lens selection thus far has used aperture-limited spectra with a blended signal from both galaxies, there is a substantial yield of lower-redshift, strongly lensing galaxies left to find (see Knabel et al. 2020, for a discussion on different lensing detection methods) and a strong motivation for machine-learning identification applied on all-sky surveys. Monitoring machine-learning-identified lensing systems (some 3000 now in total from KiDS and DES) is as effective as the entire all-sky campaign of *TESS* (Fig. 10).

The odds of finding a supernova with *TESS* are low for its primary all-sky mission, but the high cadence (30 min) and long campaign of *TESS* (27 d) would result in accurate light curves, even if these were a mix of two light curves observed in different lensed images of the source galaxy. The possibility of observing such events and the potential pay-offs of an independent Hubble constant measurement could make this a worthy additional science to be conducted with the *TESS* telescope during its extended mission. Considering the science potential for an extended mission, the potential number of supernovae to be discovered goes up commensurately, especially when a modified observing strategy is followed with longer campaigns on each sector and faster processing of each sector allows rapid successful spectroscopic and high-resolution imaging follow-up of potential supernovae.

As a first step, the existing *TESS* archive can be scoured for the signal of a multiple-lensed supernova with confirmation using multicolour ground-based surveys (e.g. SDSS or DES). If this proof of concept works, a rapid pipeline for detection of such rare events should be a priority for timely follow-up; high resolution imaging to discriminate each SN image and spectroscopy to confirm supernova type.

Alternatively, the number of strong lensing galaxies which are candidates for *TESS* monitoring will be continuously increased. This can be additional motivation for machine-learning efforts to find strong lensing galaxies at low redshift in all-sky imaging such as the DES search (Jacobs et al. 2019; Huang et al. 2020, 2021).

5.1 Ecliptic Pole monitoring

We argue that special attention should be given to the Ecliptic Poles where *TESS* has continuous coverage and JWST continuous viewing zone lies (always available for rapid follow-up). These regions are already of intense interest for transient monitoring, especially the Northern Ecliptic pole is promising for extra-galactic work (see Jansen & Windhorst 2018).

TESS has an undeniable advantage over ground-based surveys in these regions thanks to the near year-round monitoring of one of these poles. Fig. 11 shows the number of lensed supernovae one can expect in these 60 deg^2. This estimate is much simpler as *TESS* observed any particular pole 50 per cent of the time, improving the odds of observing one: a 2 per cent chance of supernova type Ia and 4 per cent chance of a core-collapse supernova each year, both in a lensed galaxy and observable with *TESS* ($m < 19$), assuming 1.2 lensing system per square degree (Fig. 10). An added benefit is that the complete light curve of the supernova is likely to be fully sampled by *TESS* alone.

In the South, much of the ecliptic pole is crowded by the Large Magellanic Cloud but the northern ecliptic pole offers both a reasonable chance of success and *JWST* continuous follow-up potential. With the northern pole unavailable for the Rubin Observatory, this gives *TESS* a unique parameter space for a potential, near-future, and high scientific return science target for its extended mission.

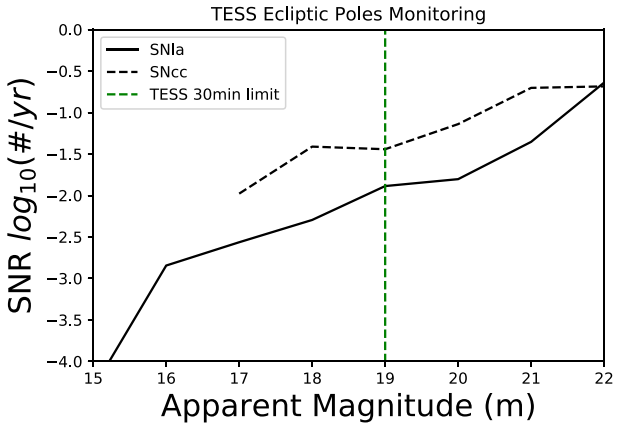

Figure 11. The estimate of number of lensed supernovae in the ecliptic poles, one of which is monitored for 357 d out of the year with *TESS*.

ACKNOWLEDGEMENTS

The material is based upon work supported by NASA Kentucky under NASA award No: NNX15AR69H. This research has made use of the NASA/IPAC Extragalactic Database (NED) which is operated by the Jet Propulsion Laboratory, California Institute of Technology, under contract with the National Aeronautics and Space Administration. This research has made use of NASA's Astrophysics Data System. This research made use of ASTROPY, a community-developed core PYTHON package for Astronomy (Astropy Collaboration 2013) and matplotlib, a PYTHON library for publication quality graphics (Hunter 2007). PyRAF is a product of the Space Telescope Science Institute, which is operated by AURA for NASA. This research made use of SciPy (Jones et al. 2001).

DATA AVAILABILITY

The data underlying this article are available in the article and in its online supplementary material (jupyter notebook).

REFERENCES

Abazajian K. et al., 2003, AJ, 126, 2081
Abolfathi B. et al., 2018, ApJS, 235, 42
Astropy Collaboration, 2013, A&A, 558, A33
Auger M. W., Treu T., Bolton A. S., Gavazzi R., Koopmans L. V. E., Marshall P. J., Bundy K., Moustakas L. A., 2009, ApJ, 705, 1099
Auger M. W., Treu T., Bolton A. S., Gavazzi R., Koopmans L. V. E., Marshall P. J., Moustakas L. A., Burles S., 2010, ApJ, 724, 511
Baldry I. K. et al., 2018, MNRAS, 474, 3875
Beaton R. L. et al., 2016, ApJ, 2, 210
Bolton A. S., Burles S., Koopmans L. V. E., Treu T., Moustakas L. A., 2006, ApJ, 638, 703
Bolton A. S., Burles S., Koopmans L. V. E., Treu T., Gavazzi R., Moustakas L. A., Wayth R., Schlegel D. J., 2008a, ApJ, 682, 964
Bolton A. S., Treu T., Koopmans L. V. E., Gavazzi R., Moustakas L. A., Burles S., Schlegel D. J., Wayth R., 2008b, ApJ, 684, 248
Dahlén T., Fransson C., 1999, A&A, 350, 349
de Jong J. T. A., Verdoes Kleijn G. A., Kuijken K. H., Valentijn E. A., 2013, Exp. Astron., 35, 25
de Jong J. T. A. et al., 2015, A&A, 582, A62
de Jong J. T. A. et al., 2017, A&A, 604, A134
Domingue D. L., Keel W. C., White R. E. III, 2000, ApJ, 545, 171
Driver S. P. et al., 2009, Astron. Geophys., 50, 050000
Gavazzi R., Treu T., Rhodes J. D., Koopmans L. V. E., Bolton A. S., Burles S., Massey R. J., Moustakas L. A., 2007, ApJ, 667, 176

Gavazzi R., Treu T., Koopmans L. V. E., Bolton A. S., Moustakas L. A., Burles S., Marshall P. J., 2008, ApJ, 677, 1046
Goldstein D. A., Nugent P. E., Goobar A., 2019, ApJS, 243, 6
Goobar A., Mörtsell E., Amanullah R., Goliath M., Bergström L., Dahlén T., 2002a, A&A, 392, 757
Goobar A., Mörtsell E., Amanullah R., Nugent P., 2002b, A&A, 393, 25
Goobar A. et al., 2017, Science, 356, 291
Grillo C. et al., 2018, ApJ, 860, 94
Holwerda B. W., 2008, MNRAS, 386, 475
Holwerda B. W., Keel W. C., 2013, A&A, 556, A42
Holwerda B. W., Keel W. C., 2016, International Astronomical Union, 11, 248
Holwerda B. W., Keel W. C., Bolton A., 2007, AJ, 134, 2385
Holwerda B. W., Keel W. C., Williams B., Dalcanton J. J., de Jong R. S., 2009, AJ, 137, 3000
Holwerda B. W., Böker T., Dalcanton J. J., Keel W. C., de Jong R. S., 2013, MNRAS, 433, 47
Holwerda B. W., Reynolds A., Smith M., Kraan-Korteweg R. C., 2015a, MNRAS, 446, 3768
Holwerda B. W. et al., 2015b, MNRAS, 449, 4277
Holwerda B. W., Keel W. C., Kenworthy M. A., Mack K. J., 2015c, MNRAS, 451, 2390
Holz D. E., 2001, ApJ, 556, L71
Huang X. et al., 2020, ApJ, 894, 78
Huang X. et al., 2021, ApJ, 909, 27
Hunter J. D., 2007, Comput. Sci. Eng., 9, 90
Jacobs C. et al., 2019, ApJS, 243, 17
Jansen R. A., Windhorst R. A., 2018, PASP, 130, 124001
Jones E., Oliphant T., Peterson P. et al., 2001, Nature Methods, 17, 261
Keel W. C., White R. E. III, 2001a, AJ, 121, 1442
Keel W. C., White R. E. III, 2001b, AJ, 122, 1369
Kelly P. L., Filippenko A. V., Burke D. L., Hicken M., Ganeshalingam M., Zheng W., 2015a, Science, 347, 1459
Kelly P. L. et al., 2015b, Science, 347, 1123
Kelly P. L. et al., 2015c, Astron. Telegram, 8402, 1
Knabel S. et al., 2020, AJ, 160, 223
Koopmans L. V. E., Treu T., Bolton A. S., Burles S., Moustakas L. A., 2006, ApJ, 649, 599
Kostrzewa-Rutkowska Z., Wyrzykowski Ł., Jaroszyński M., 2013, MNRAS, 429, 2392
Li W. et al., 2011, MNRAS, 412, 1441
Li R. et al., 2020, ApJ, 899, 30
Liao K., 2018, preprint (arXiv:1812.03408)
Lintott C. J. et al., 2008, MNRAS, 389, 1179
Liske J. et al., 2015, MNRAS, 452, 2087
Newton E. R., Marshall P. J., Treu T., Auger M. W., Gavazzi R., Bolton A. S., Koopmans L. V. E., Moustakas L. A., 2011, ApJ, 734, 104
Oguri M., 2010, PASJ, 62, 1017
Oguri M., 2019, Rep. Prog. Phys., 82, 126901
Oguri M., Marshall P. J., 2010, MNRAS, 405, 2579
Petrillo C. E. et al., 2017, MNRAS, 472, 1129
Petrillo C. E. et al., 2018, MNRAS, 482, 807
Petrillo C. E. et al., 2019, MNRAS, 484, 3879
Petrushevska T., Okamura T., Kawamata R., Hangard L., Mahler G., Goobar A., 2018, Astron. Rep., 62, 917
Pierel J. D. R., Rodney S., 2019, ApJ, 876, 107
Planck CollaborationVI, 2020, A&A, 641, 6P
Porciani C., Madau P., 2000, ApJ, 532, 679
Quimby R. M. et al., 2014, Science, 344, 396
Refsdal S., 1964, MNRAS, 128, 307
Richardson D. R. L. J. III, Wright J., Maddox L., 2014, AJ, 147, 118
Ricker G. R. et al., 2015, J. Astron. Telesc., Instrum. Syst., 1, 014003
Riess A. G., 2019, Nat. Rev. Phys., 2, 10
Riess A. G. et al., 2016, ApJ, 826, 56
Riess A. G. et al., 2018, ApJ, 853, 126
Shu Y. et al., 2015, ApJ, 803, 71
Shu Y., Bolton A. S., Mao S., Kang X., Li G., Soraisam M., 2018, ApJ, 864, 91
Strolger L.-G. et al., 2015, ApJ, 813, 93
Treu T., Marshall P. J., 2016, A&A Rev., 24, 11
Treu T., Koopmans L. V., Bolton A. S., Burles S., Moustakas L. A., 2006, ApJ, 640, 662
Treu T., Gavazzi R., Gorecki A., Marshall P. J., Koopmans L. V. E., Bolton A. S., Moustakas L. A., Burles S., 2009, ApJ, 690, 670
Tu Z. L., Hu J., Wang F. Y., 2019, MNRAS, 484, 4337
Vallely P. J. et al., 2019, MNRAS, 487, 2372
Vega-Ferrero J., Diego J. M., Miranda V., Bernstein G. M., 2018, ApJ, 853, L31
Wang Y., 2000, ApJ, 531, 676
White R. E. III, Keel W. C., Conselice C. J., 2000, ApJ, 542, 761
Williams L. L. R., Liesenborgs J., 2019, MNRAS, 482, 5666
Wojtak R., Hjorth J., Gall C., 2019, MNRAS, 487, 3342

This paper has been typeset from a TEX/LATEX file prepared by the author.